JOURNAL OF GUIDANCE, CONTROL, AND DYNAMICS
Vol. 32, No. 6, November–December 2009

Model Development and Code Verification for Simulation of Electrodynamic Tether System

Joshua R. Ellis* and Christopher D. Hall†
Virginia Polytechnic Institute and State University, Blacksburg, Virginia 24061-0203

DOI: 10.2514/1.44638

We develop a numerical model of an electrodynamic tether system composed of two finite end bodies and a flexible tether. The equations of motion of the system are presented along with two methods of discretizing the partial differential equations governing the tether vibrations. The first method is the assumed modes method in which the tether displacements are represented as series of generalized coordinates and assumed mode functions, and the second is a finite element method in which displacements and slopes at points along the tether are interpolated by shape functions. The method of manufactured solutions is used to verify that the computer codes written to simulate the system motion implement the discretization methods properly. Both the assumed modes method and the finite element method perform well for relatively low discretization levels; however, as the number of longitudinal assumed modes is increased, the mass matrix for the longitudinal vibrations becomes poorly conditioned, resulting in numerical errors that can cause the tether vibrations to improperly diverge. This behavior is not seen in the finite element method because the mass matrices for both the transverse and longitudinal vibrations are always well-conditioned.

Nomenclature

$\mathcal{A}$	=	main end body
A_{Mki}	=	assumed-modes-method forcing-vector elements, $m^2 \cdot s^{-2}$
$\mathbf{A}_T$	=	acceleration vector used in derivation of tether displacement equations, $m \cdot s^{-2}$
A_{Ti}	=	components of $\mathbf{A}_T$ expressed in $\mathcal{F}_E$, $m \cdot s^{-2}$
a	=	semimajor axis, m
a_{Di}	=	disturbance acceleration components expressed in $\mathcal{F}_O$, $m \cdot s^{-2}$
$\mathbf{B}$	=	central-body magnetic field vector, T
$\mathbf{B}_L$	=	acceleration vector used in determining tether libration equations of motion, $m \cdot s^{-2}$
B_{Li}	=	components of $\mathbf{B}_L$ expressed in $\mathcal{F}_E$, $m \cdot s^{-2}$
$\mathcal{B}$	=	secondary end body
C_{ij}	=	tether displacement generalized coordinates or degrees of freedom, m
$C_{\Delta h}$, $C_{\Delta t}$	=	constants in discretization error expression
c	=	structural damping constant, s
$d\bar{s}$	=	differential unstretched tether element
EA	=	longitudinal stiffness of the tether, N
e	=	eccentricity
$\mathbf{e}$	=	set of osculating orbit elements
$\hat{\mathbf{e}}_i$	=	unit axes of $\mathcal{F}_E$
$\mathcal{F}_A$	=	$\mathcal{A}$ body frame
$\mathcal{F}_B$	=	$\mathcal{B}$ body frame
$\mathcal{F}_E$	=	tether-fixed frame
$\mathcal{F}_N$	=	inertial frame
$\mathcal{F}_O$	=	orbital frame
f, F	=	numerical and exact solutions to a set of partial differential equations
$\mathbf{f}_T$, $\mathbf{f}_L$	=	manufactured solution vectors, $m/s^2 m^2 \cdot s^{-2}$
$\mathbf{f}_i$	=	finite element method external force vector, m/s^2
G_A	=	mass center of $\mathcal{A}$
G_B	=	mass center of $\mathcal{B}$
$\mathbf{g}_i$	=	finite element method gravity vector, $m^2 \cdot s^{-2}$
h	=	specific angular momentum, $m^2 \cdot s^{-1}$
I	=	inclination, deg
$\mathbf{I}_A$	=	centroidal moment of inertia tensor of $\mathcal{A}$, $kg \cdot m^2$
$\mathbf{I}_B$	=	centroidal moment of inertia tensor of $\mathcal{B}$, $kg \cdot m^2$
i	=	current in the tether, A
L	=	unstretched length of the tether, m
l	=	orbit parameter, m
ℓ_e	=	length of finite element, m
M_{ij}	=	finite element method mass matrix elements, m
$M_{k,ij}$	=	assumed-modes-method mass matrix elements, m
m_A	=	mass of $\mathcal{A}$, kg
m_B	=	mass of $\mathcal{B}$, kg
N_e	=	number of finite elements
N_i	=	finite element method global shape function
N_i^e	=	finite element method element shape function
N_{ij}	=	tether assumed mode functions
N_L	=	number of longitudinal assumed modes
N_T	=	number of transverse assumed modes
n	=	number of degrees of freedom for each tether displacement in the finite element method
$\hat{\mathbf{n}}_i$	=	unit axes of $\mathcal{F}_N$
O	=	inertial origin
$\hat{\mathbf{o}}_i$	=	unit axes of $\mathcal{F}_O$
P_A	=	tether attachment point on $\mathcal{A}$
P_B	=	tether attachment point on $\mathcal{B}$
p	=	spatial order of accuracy
$\mathbf{p}_A$	=	tether attachment vector on $\mathcal{A}$, m
$\mathbf{p}_B$	=	tether attachment vector on $\mathcal{B}$, m
q	=	temporal order of accuracy
$\mathbf{R}_T(\bar{s}, t)$	=	position vector of $d\bar{s}$ relative to O, m
r	=	discretization refinement factor
$\mathbf{r}$	=	position vector of $d\bar{s}$ relative to P_A
r_A	=	orbital radius of G_A, m
$\mathbf{r}_A$	=	position vector of G_A, m
$\mathbf{r}_B$	=	position vector of G_B, m
r_L	=	distance between P_B and P_A, m
$\mathbf{r}_L$	=	position vector of P_B relative to P_A, m
$\bar{s}$	=	tether unstretched arc length, m
$\bar{s}_0$, $\bar{s}_f$	=	value of $\bar{s}$ at the beginning an end of a finite element, m

Presented at the 18th AAS/AIAA Spaceflight Mechanics Meeting, Galveston, TX, 27–31 January 2008; received 9 April 2009; revision received 22 July 2009; accepted for publication 22 July 2009.

*Graduate Student, Aerospace and Ocean Engineering Department; joellis3@vt.edu.

†Professor, Aerospace and Ocean Engineering Department.

$\mathbf{T}(\bar{s}, t)$ = tension vector in the tether, N
t = time, s
$u(\bar{s}, t)$ = tether transverse displacement in the $\hat{\mathbf{e}}_1$ direction, m
$\hat{\mathbf{u}}$ = unit dipole axis
$v(\bar{s}, t)$ = tether transverse displacement in the $\hat{\mathbf{e}}_2$ direction, m
$w(\bar{s}, t)$ = tether transverse displacement in the $\hat{\mathbf{e}}_3$ direction, m
α = in-plane tether libration angle, deg
β = out-of-plane tether libration angle, deg
γ_{ki} = finite element method parameters, m
Δh, Δt = measures of spatial and temporal discretization
$\varepsilon(\bar{s}, t)$ = strain in the tether
ϵ = discretization error
μ = gravitational parameter of the central body, $\mathrm{m}^3 \cdot \mathrm{s}^{-2}$
μ_M = dipole strength, $\mathrm{T} \cdot \mathrm{m}^3$
ν = true anomaly, deg
ξ = finite element natural coordinate
$\bar{\rho}$ = linear mass density of the unstretched tether, $\mathrm{kg} \cdot \mathrm{m}$
$\hat{\boldsymbol{\tau}}$ = tether unit tangent vector
Ω = right ascension of the ascending node, deg
ω = argument of periapsis, deg
$\boldsymbol{\omega}_{A/N}$ = angular velocity of $\mathcal{F}_A$ relative to $\mathcal{F}_N$, $\mathrm{rad} \cdot \mathrm{s}^{-1}$
$\boldsymbol{\omega}_{B/N}$ = angular velocity of $\mathcal{F}_B$ relative to $\mathcal{F}_N$, $\mathrm{rad} \cdot \mathrm{s}^{-1}$
$\boldsymbol{\omega}_{E/N}$ = angular velocity of $\mathcal{F}_E$ relative to $\mathcal{F}_N$, $\mathrm{rad} \cdot \mathrm{s}^{-1}$
$\boldsymbol{\omega}_{E/O}$ = angular velocity of $\mathcal{F}_E$ relative to $\mathcal{F}_O$, $\mathrm{rad} \cdot \mathrm{s}^{-1}$
$\boldsymbol{\omega}_{O/N}$ = angular velocity of $\mathcal{F}_O$ relative to $\mathcal{F}_N$, $\mathrm{rad} \cdot \mathrm{s}^{-1}$
$\mathbf{0}$ = zero vector
$\cdot$ = time derivative
$^{\circ}$ = time derivative as seen by $\mathcal{F}_E$

Superscript

$*$ = manufactured solution

I. Introduction

IN RECENT years, electrodynamic tethers (EDTs) have been proposed for a number of space applications. An EDT is a long, thin, conductive tether in orbit around a body with a strong magnetic field. The body is typically Earth, but EDTs have been proposed for a number of Jupiter-based missions as well. As the tether moves in its orbit through the magnetic field of the central body, an electrical potential is induced across its ends. If the ends of the tether are allowed to make electrical contact with the ambient plasma environment, this electrical potential will drive a current through the tether that interacts with the magnetic field to produce a distributed force along the tether. In this manner, an EDT can generate propulsion without the need for propellant. Decreases in magnetic field strength at higher orbit altitudes limit the operational regime of EDTs to low Earth orbit (LEO); however, EDTs in LEO can be used for a number of useful applications, such as debris removal [1–3], orbital maintenance of the International Space Station [4], and orbital maneuvering of satellites. One of the more promising proposed EDT missions is NASA's momentum-exchange electrodynamic reboost (MXER) tether system [5], which has been proposed for transferring satellites from LEO to much higher orbits such as geosynchronous transfer orbits and escape trajectories.

In general, the research conducted on the dynamics and control of EDTs can be divided into two main categories. The first category deals with the effects of the electrodynamic force on the orbit of the system and how the current in the tether can be modulated to produce a desired change in the orbit of the system [6,7]. The second category deals with the librational and vibrational motions of the tether induced by the electrodynamic force [8–10]. The principal result of this category of research is that both the tether librations and the flexible oscillations of the tether are inherently unstable due to a constant pumping of energy into the system by the electrodynamic force. Two excellent books that contain a great deal of analytical work on the dynamics and control of EDT systems are those by Beletsky and Levin [11], and Levin [12]. Also, a detailed literature review of the dynamics and control of EDT systems can be found in the introduction of [13].

One practice common to virtually all of the research previously conducted on EDT dynamics and control is the introduction of various simplifications into the system model. These simplifications include modeling the end bodies as point masses and the tether as a rigid rod, constraining the motion of some part of the system to a Keplerian orbit, and modeling the magnetic field as a nontilted, nonrotating dipole. Such assumptions greatly simplify the system equations of motion and allow for the derivation of analytical results; however, these simplifications also remove important dynamics from the system, such as the flexible oscillations of the tether and the attitude motion of the end bodies. In light of this fact, the goal of this research is to develop a numerical model of an EDT system that contains as few simplifying assumptions as possible. Such a numerical model will be able to generate accurate long-term predictions of EDT dynamics that analytical results based upon simplified models cannot necessarily provide. Thus, we consider an EDT system composed of two rigid end bodies connected by a flexible tether. The end bodies are allowed to undergo full three-dimensional translational and rotational motions, and the tether is allowed to experience transverse and longitudinal nonlinear oscillations. The magnetic field is modeled as a tilted dipole that is fixed to the central body as it rotates. The model presented in this paper is a variation of the model presented in [13]. The principal difference between the two models is that in this work the state of one of the end bodies is parameterized by a set of osculating classical orbit elements, whereas in [13] a set of spherical coordinates is used.

Because the system model we consider treats the tether as a flexible continuum, the equations of motion of the tether are partial differential equations (PDEs) that must be discretized to generate a numerical solution. We use two different discretization methods for the equations of motion of the tether. The first method is the assumed modes method (AMM), in which the displacements of the tether away from its unstretched state are represented as finite sums of generalized coordinates and assumed mode functions. The second method is a finite element method (FEM), in which displacements and slopes at points along the tether are interpolated by shape functions. For both methods, the Galerkin method is used to convert the governing PDEs into a finite set of ordinary differential equations (ODEs).

Both the assumed modes and finite element methods have been used previously to study the dynamics of both electrodynamic [13,14] and nonelectrodynamic tether systems [15,16]. The coding of the discretized equations of motion is a nontrivial task, and a wide variety of mistakes can be made in the coding process. In spite of this fact, evidence is rarely presented to show that the discretized equations of motion have been coded properly and that the resulting numerical solutions provide accurate approximations to solutions of the governing partial differential equations. Pradhan et al. [15] monitored the total energy of a conservative nonelectrodynamic tether system in which the PDEs were discretized using assumed modes. Because the system was conservative, the authors used the fact that the total energy remained relatively constant during simulations to verify their solutions. Frequencies of the lower-order modes of the tether were also compared with results from previous research as a means of verification. A similar energy-check strategy could be applied to an EDT system by including the total system energy as an additional state and using work-energy relations to predict how the energy should evolve with time. Comparing this energy time history with one calculated in postprocessing using the remaining state time histories could serve as a means of verification, in that the two should be in close agreement.

In this work, we use a more rigorous approach to code verification that is more commonly used in computational fluid dynamics: the method of manufactured solutions (MMS) [17,18]. In the MMS, additional terms are introduced into the governing PDEs that force a desired exact solution. Approximate solutions to this modified set of equations, calculated on increasing levels of discretization refinement, are compared with the known exact solution, and the errors between the approximate and exact solutions should decrease toward zero as the discretization is refined. If the errors decrease as they should, then the discretized equations of motion have been coded

properly and the terms introduced to manufacture the exact solution can simply be removed. At the end of this process, one can be certain that the code produces accurate approximations of the solution to the original PDEs if the discretization is sufficiently fine.

The remainder of this paper is organized as follows. In Sec. II, the EDT system model and equations of motion are presented, along with the AMM and FEM discretization procedures for the tether PDEs. The code verification procedure using the MMS is applied to both discretization methods in Sec. III, and a comparison of the two discretization methods is presented in Sec. IV.

II. System Model, Equations of Motion, and Discretization Methods

In this section we present a brief derivation of the equations of motion of the EDT system following the derivation presented in [13]. However, we note that in this model, the orbital motion of the system is parameterized using a set of osculating classical orbit elements, whereas spherical coordinates are used in [13]. We also present two discretization methods for the PDEs governing the tether vibrations. The first method is the assumed modes method, in which the tether displacements are expanded in series of time-dependent generalized coordinates and spatially dependent assumed mode functions. The Galerkin method is used to convert the PDEs into a finite set of ODEs for the generalized coordinates. The second discretization method is a finite element method using cubic Hermite polynomials that interpolate the tether displacements and slopes at points along the tether. As with the AMM, the Galerkin method is used to convert the governing PDEs into a set of finite ODEs for the tether displacements and slopes.

The EDT system considered in this study is shown in Fig. 1. The system consists of two finite rigid end bodies denoted as $\mathcal{A}$ and $\mathcal{B}$ and a flexible tether that is free to undergo both transverse and longitudinal nonlinear vibrations. The magnetic field is modeled as a tilted dipole that is fixed to the central body as it rotates, meaning that the dipole axis of the field rotates with the central body. The inertial origin O is located at the center of the central body, and the mass center of $\mathcal{A}$ (G_A) is located relative to O by the vector $\mathbf{r}_A$. The tether attaches to $\mathcal{A}$ at point P_A, which is located relative to G_A by the vector $\mathbf{p}_A$. The position of the tether relative to P_A is parameterized by the unstretched arc length along the tether, $\bar{s} \in [0, L]$, and the position of an unstretched differential tether element $\mathrm{d}\bar{s}$ relative to P_A is $\mathbf{r} = \mathbf{r}(\bar{s}, t)$. The tether attaches to $\mathcal{B}$ at point P_B, which is located relative to the mass center of $\mathcal{B}$ (G_B) by the vector $\mathbf{p}_B$.

A. Equations of Motion

As shown in [13], the translational equations of motion of the end bodies are

$$m_A \ddot{\mathbf{r}}_A = -\frac{m_A \mu}{\|\mathbf{r}_A\|^3}\mathbf{r}_A + \mathbf{T}(0,t) \tag{1}$$

$$m_B \ddot{\mathbf{r}}_B = -\frac{m_B \mu}{\|\mathbf{r}_B\|^3}\mathbf{r}_B - \mathbf{T}(L,t) \tag{2}$$

and the rotational equations of motion of the end bodies are

$$\mathbf{I}_A \cdot \dot{\boldsymbol{\omega}}_{A/N} + \boldsymbol{\omega}_{A/N} \times \mathbf{I}_A \cdot \boldsymbol{\omega}_{A/N} = \frac{3\mu}{\|\mathbf{r}_A\|^5}\mathbf{r}_A \times \mathbf{I}_A \cdot \mathbf{r}_A + \mathbf{p}_A \times \mathbf{T}(0,t) \tag{3}$$

$$\mathbf{I}_B \cdot \dot{\boldsymbol{\omega}}_{B/N} + \boldsymbol{\omega}_{B/N} \times \mathbf{I}_B \cdot \boldsymbol{\omega}_{B/N} = \frac{3\mu}{\|\mathbf{r}_B\|^5}\mathbf{r}_B \times \mathbf{I}_B \cdot \mathbf{r}_B - \mathbf{p}_B \times \mathbf{T}(L,t) \tag{4}$$

Note that we have used a first-order approximation of the gravity-gradient torque acting on each end body.

The state of G_A is parameterized by a set of osculating classical orbit elements, $\mathbf{e} = \{\, a \quad e \quad \Omega \quad I \quad \omega \quad \nu \,\}^T$. The orbital frame of the osculating orbit, $\mathcal{F}_O$, is defined such that $\hat{\mathbf{o}}_3$ points from O to G_A, $\hat{\mathbf{o}}_2$ is in the direction of the angular momentum vector of the osculating orbit, and $\hat{\mathbf{o}}_1$ completes the right-handed triad. The inertial and orbital frames are related by a 3-1-3 rotation sequence through the angles Ω, I, and $\omega + \nu$, followed by a permutation to align the axes in the proper directions. The angular velocity and acceleration of $\mathcal{F}_O$ relative to inertial are

$$\boldsymbol{\omega}_{O/N} = \frac{\sqrt{\mu l}}{r_A^2}\hat{\mathbf{o}}_2 \tag{5}$$

$$\dot{\boldsymbol{\omega}}_{O/N} = -\frac{2\mu e \sin\nu}{r_A^3}\hat{\mathbf{o}}_2 \tag{6}$$

where $l = a(1 - e^2)$ and $r_A = l/(1 + e\cos\nu)$. The Gauss form of the variational equations govern the evolution of $\mathbf{e}$:

$$\dot{a} = \frac{2a^2}{h}\left[(e\sin\nu)a_{D3} + \left(\frac{l}{r_A}\right)a_{D1}\right] \tag{7}$$

$$\dot{e} = \frac{(l\sin\nu)a_{D3} + [(l + r_A)\cos\nu + r_A e]a_{D1}}{h} \tag{8}$$

$$\dot{I} = \frac{r_A \cos(\omega + \nu)a_{D2}}{h} \tag{9}$$

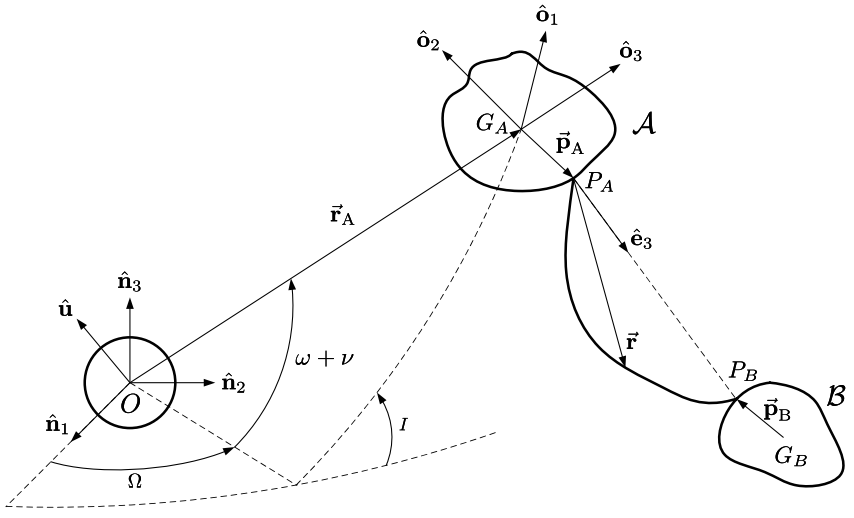

Fig. 1 Diagram of EDT system.

$$\dot{\Omega} = \frac{r_A \sin(\omega + \nu) a_{D2}}{h \sin I} \tag{10}$$

$$\dot{\omega} = \frac{-(l \cos \nu) a_{D3} + [(l + r_A) \sin \nu] a_{D1}}{he} - \frac{[r_A \sin(\omega + \nu) \cos I] a_{D2}}{h \sin I} \tag{11}$$

$$\dot{\nu} = \frac{h}{r_A^2} + \frac{(l \cos \nu) a_{D3} - [(l + r_A) \sin \nu] a_{D1}}{he} \tag{12}$$

where $h = \sqrt{\mu l}$. Note that the disturbance acceleration components must be expressed relative to $\mathcal{F}_O$.

Define the tether-fixed frame $\mathcal{F}_E$ relative to $\mathcal{F}_O$ by a 2-1 rotation sequence through the angles α and $-\beta$ such that $\hat{\mathbf{e}}_3$ points from P_A to P_B. Note that the angles α and β are the in- and out-of-plane libration angles of the tether relative to $\mathcal{F}_O$. The angular velocity of $\mathcal{F}_E$ relative to $\mathcal{F}_O$ is

$$\boldsymbol{\omega}_{E/O} = -\dot{\beta} \hat{\mathbf{e}}_1 + \dot{\alpha} \cos \beta \hat{\mathbf{e}}_2 + \dot{\alpha} \sin \beta \hat{\mathbf{e}}_3 \tag{13}$$

The equations of motion of α and β are derived from the equation of motion of $\mathcal{B}$ as [13]

$$\ddot{\alpha} = \frac{1}{\cos \beta} \left[\frac{B_{L1}}{r_L} + \dot{\alpha} \dot{\beta} \sin \beta \right] \tag{14}$$

$$\ddot{\beta} = \frac{B_{L2}}{r_L} \tag{15}$$

where the vector $\mathbf{B}_L$ is defined as

$$\begin{aligned} \mathbf{B}_L = &- \frac{\mu}{\|\mathbf{r}_B\|^3} \mathbf{r}_B - \frac{\mathbf{T}(L,t)}{m_B} - \ddot{\mathbf{r}}_A - \ddot{\mathbf{p}}_A + \ddot{\mathbf{p}}_B \\ &- (\dot{\boldsymbol{\omega}}_{O/N} + \boldsymbol{\omega}_{O/N} \times \boldsymbol{\omega}_{E/O}) \times \mathbf{r}(L,t) \\ &- \boldsymbol{\omega}_{E/N} \times [\boldsymbol{\omega}_{E/N} \times \mathbf{r}(L,t)] - 2\boldsymbol{\omega}_{E/N} \times \mathring{\mathbf{r}}(L,t) \end{aligned} \tag{16}$$

Let $\mathbf{R}_T = \mathbf{r}_A + \mathbf{p}_A + \mathbf{r}$ be the position of $\mathrm{d}\bar{s}$ relative to O. Then, following [13], the equation of motion of the tether is

$$\ddot{\mathbf{r}} = -\frac{\mu}{\|\mathbf{R}_T\|^3} \mathbf{R}_T + \frac{1}{\bar{\rho}} \frac{\partial \mathbf{T}}{\partial \bar{s}} + \frac{i}{\bar{\rho}} \frac{\partial \mathbf{r}}{\partial \bar{s}} \times \mathbf{B} - \ddot{\mathbf{r}}_A - \ddot{\mathbf{p}}_A \tag{17}$$

Note that Eq. (17) is a PDE in terms of time and the spatial coordinate $\bar{s}$. The geometric boundary conditions of Eq. (17) are

$$\mathbf{r}(0,t) = \mathbf{0} \tag{18}$$

$$\mathbf{r}(L,t) = r_L \hat{\mathbf{e}}_3 \tag{19}$$

The tension in the tether is modeled using the linear Kelvin–Voigt law of viscoelasticity:

$$\mathbf{T} = EA(\varepsilon + c\dot{\varepsilon}) \hat{\boldsymbol{\tau}} \tag{20}$$

where the strain and tether unit tangent vector are given by

$$\varepsilon = \left\| \frac{\partial \mathbf{r}}{\partial \bar{s}} \right\| - 1 \tag{21}$$

$$\hat{\boldsymbol{\tau}} = \frac{\partial \mathbf{r} / \partial \bar{s}}{\|\partial \mathbf{r} / \partial \bar{s}\|} \tag{22}$$

Because the magnetic field is modeled as a dipole, the magnetic field vector at $\mathrm{d}\bar{s}$ is

$$\mathbf{B} = \frac{\mu_M}{\|\mathbf{R}_T\|^3} \left[\hat{\mathbf{u}} - \frac{3(\hat{\mathbf{u}} \cdot \mathbf{R}_T) \mathbf{R}_T}{\|\mathbf{R}_T\|^2} \right] \tag{23}$$

Note that $\hat{\mathbf{u}}$ is time-varying because the field is tilted relative to the spin axis of the central body and fixed to the rotating central body.

The first step in the discretization of Eq. (17) is to express the position of the tether relative to P_A as

$$\mathbf{r} = u(\bar{s},t) \hat{\mathbf{e}}_1 + v(\bar{s},t) \hat{\mathbf{e}}_2 + [\bar{s} + w(\bar{s},t)] \hat{\mathbf{e}}_3 \tag{24}$$

Note that when the tether is completely unstretched ($u = v = w = 0$) it lies along $\hat{\mathbf{e}}_3$, which defines the line connecting P_A and P_B. In the following subsections, we present two different methods for converting Eqs. (17) and (24) into a finite set of ODEs.

B. Discretization Using the Assumed Modes Method

In the AMM discretization we first expand the left-hand side of Eq. (17) to obtain

$$\begin{aligned} \mathring{\mathbf{r}} = &- \frac{\mu}{\|\mathbf{R}_T\|^3} \mathbf{R}_T + \frac{1}{\bar{\rho}} \frac{\partial \mathbf{T}}{\partial \bar{s}} + \frac{i}{\bar{\rho}} \frac{\partial \mathbf{r}}{\partial \bar{s}} \times \mathbf{B} - \ddot{\mathbf{r}}_A - \ddot{\mathbf{p}}_A - \dot{\boldsymbol{\omega}}_{E/N} \times \mathbf{r} \\ &- \boldsymbol{\omega}_{E/N} \times (\boldsymbol{\omega}_{E/N} \times \mathbf{r}) - 2\boldsymbol{\omega}_{E/N} \times \mathring{\mathbf{r}} = \mathbf{A}_T \end{aligned} \tag{25}$$

Combining Eqs. (24) and (25), the equations of motion for the tether displacements are

$$\ddot{u} = A_{T1} \tag{26}$$

$$\ddot{v} = A_{T2} \tag{27}$$

$$\ddot{w} = A_{T3} \tag{28}$$

Next, assume that the tether displacements are equal to finite sums of products of time-dependent generalized coordinates $C_{ij}(t)$ and spatially dependent assumed mode functions $N_{ij}(\bar{s})$:

$$u(\bar{s},t) = \sum_{j=1}^{N_T} C_{1j}(t) N_{1j}(\bar{s}) \tag{29}$$

$$v(\bar{s},t) = \sum_{j=1}^{N_T} C_{2j}(t) N_{2j}(\bar{s}) \tag{30}$$

$$w(\bar{s},t) = \sum_{j=1}^{N_L} C_{3j}(t) N_{3j}(\bar{s}) \tag{31}$$

Note that the numbers of transverse and longitudinal assumed modes can be different. The only constraints on the assumed mode functions are that they form a linearly independent complete set and that they satisfy the geometric boundary conditions of the tether PDEs [19]. Substituting Eqs. (29) and (30) into Eqs. (26) and (27) and applying the Galerkin method, we obtain the following set of $2N_T$ ODEs for the transverse generalized coordinates:

$$\sum_{j=1}^{N_T} M_{1,ij} \ddot{C}_{1j} = A_{M1i}, \qquad i = 1, \ldots, N_T \tag{32}$$

$$\sum_{j=1}^{N_T} M_{2,ij} \ddot{C}_{2j} = A_{M2i}, \qquad i = 1, \ldots, N_T \tag{33}$$

where we have defined

$$M_{1,ij} = \int_0^L N_{1i}(\bar{s}) N_{1j}(\bar{s}) \, \mathrm{d}\bar{s} \tag{34}$$

$$M_{2,ij} = \int_0^L N_{2i}(\bar{s}) N_{2j}(\bar{s}) \, \mathrm{d}\bar{s} \tag{35}$$

$$A_{M1i} = \int_0^L A_{T1} N_{1i}(\bar{s})\, \mathrm{d}\bar{s} \tag{36}$$

$$A_{M2i} = \int_0^L A_{T2} N_{2i}(\bar{s})\, \mathrm{d}\bar{s} \tag{37}$$

To discretize Eq. (28), first define the dynamic boundary condition of the tether as

$$\ddot{w}(L, t) = B_{L3} \tag{38}$$

Equation (38) is derived from the translational equation of motion of $\mathcal{B}$ and defines how the longitudinal displacement at P_B varies with time [13]. Substituting Eq. (31) into Eqs. (28) and (38) and applying the Galerkin method, we obtain the following set of N_L ODEs for the longitudinal generalized coordinates:

$$\sum_{j=1}^{N_L} M_{3,ij} \ddot{C}_{3j} = A_{M3i}, \qquad i = 1, \ldots, N_L - 1 \tag{39}$$

$$\sum_{j=1}^{N_L} \ddot{C}_{3j} N_{3j}(L) = B_{L3} \tag{40}$$

where we have defined

$$M_{3,ij} = \int_0^L N_{3i}(\bar{s}) N_{3j}(\bar{s})\, \mathrm{d}\bar{s} \tag{41}$$

$$A_{M3i} = \int_0^L A_{T3} N_{3i}(\bar{s})\, \mathrm{d}\bar{s} \tag{42}$$

Note that Eq. (38) is used as one of the equations of motion for the longitudinal generalized coordinates because it introduces the dynamic boundary condition of the tether into the discretized equations of motion.

Equations (32), (33), (39), and (40) define a set of $2N_T + N_L$ ODEs for the tether generalized coordinates. These ODEs are solved in combination with the ODEs governing the translational and rotational motions of the end bodies and the librational motion of the tether to obtain a numerical solution for the system motion. In this work, the assumed mode functions are taken as

$$N_{1j}(\bar{s}) = \sqrt{2} \sin\left(\frac{j\pi}{L}\bar{s}\right) \tag{43}$$

$$N_{2j}(\bar{s}) = \sqrt{2} \sin\left(\frac{j\pi}{L}\bar{s}\right) \tag{44}$$

$$N_{3j}(\bar{s}) = \left(\frac{\bar{s}}{L}\right)^j \tag{45}$$

which satisfy all of the geometric boundary conditions of the tether. Note that the transverse assumed mode functions are orthogonal, and so $M_{1,ij} = M_{2,ij} = 0$ for $i \neq j$.

C. Discretization Using the Finite Element Method

In the FEM discretization we begin by rewriting Eq. (17) in the weak form [20]. Applying the Galerkin method to Eq. (17), we obtain

$$\int_0^L \ddot{\mathbf{r}} N_i(\bar{s})\, \mathrm{d}\bar{s} = \int_0^L \left(-\frac{\mu}{\|\mathbf{R}_T\|^3}\mathbf{R}_T + \frac{1}{\bar{\rho}}\frac{\partial \mathbf{T}}{\partial \bar{s}} + \frac{i}{\bar{\rho}}\frac{\partial \mathbf{r}}{\partial \bar{s}} \times \mathbf{B} - \ddot{\mathbf{r}}_A - \ddot{\mathbf{p}}_A \right) N_i(\bar{s})\, \mathrm{d}\bar{s} \tag{46}$$

where N_i is defined over the entire length of the tether. Note the difference between the way in which the Galerkin method is applied here and in the AMM: in the AMM, different shape functions are used as the weighting functions for the transverse and longitudinal tether equations of motion, whereas the same shape function is used here as the weighting function for the equations of motion of all three tether displacements. Integrating the tension term by parts and introducing the translational equations of motion of the end bodies, Eq. (46) is rewritten as

$$\int_0^L \ddot{\mathbf{r}} N_i(\bar{s})\, \mathrm{d}\bar{s} + \frac{m_B}{\bar{\rho}} \ddot{\mathbf{r}}_L N_i(L) = -\gamma_{1i}\ddot{\mathbf{r}}_A - \gamma_{2i}\ddot{\mathbf{p}}_A + \gamma_{3i}\ddot{\mathbf{p}}_B + \mathbf{g}_i + \mathbf{f}_i \tag{47}$$

where we have defined the quantities

$$\gamma_{1i} = \int_0^L N_i(\bar{s})\, \mathrm{d}\bar{s} + \frac{m_B}{\bar{\rho}} N_i(L) + \frac{m_A}{\bar{\rho}} N_i(0) \tag{48}$$

$$\gamma_{2i} = \int_0^L N_i(\bar{s})\, \mathrm{d}\bar{s} + \frac{m_B}{\bar{\rho}} N_i(L) \tag{49}$$

$$\gamma_{3i} = \frac{m_B}{\bar{\rho}} N_i(L) \tag{50}$$

$$\mathbf{g}_i = -\mu \left[\int_0^L \frac{\mathbf{R}_T}{\|\mathbf{R}_T\|^3} N_i(\bar{s})\, \mathrm{d}\bar{s} + \frac{m_B}{\bar{\rho}} \frac{\mathbf{r}_B}{\|\mathbf{r}_B\|^3} N_i(L) + \frac{m_A}{\bar{\rho}} \frac{\mathbf{r}_A}{\|\mathbf{r}_A\|^3} N_i(0) \right] \tag{51}$$

$$\mathbf{f}_i = -\frac{1}{\bar{\rho}} \int_0^L \mathbf{T} \frac{\mathrm{d}N_i(\bar{s})}{\mathrm{d}\bar{s}}\, \mathrm{d}\bar{s} + \frac{i}{\bar{\rho}} \int_0^L \frac{\partial \mathbf{r}}{\partial \bar{s}} \times \mathbf{B} N_i(\bar{s})\, \mathrm{d}\bar{s} \tag{52}$$

Next, express the tether displacements as

$$u(\bar{s}, t) = \sum_{j=1}^{n} C_{1j}(t) N_j(\bar{s}) \tag{53}$$

$$v(\bar{s}, t) = \sum_{j=1}^{n} C_{2j}(t) N_j(\bar{s}) \tag{54}$$

$$w(\bar{s}, t) = \sum_{j=1}^{n} C_{3j}(t) N_j(\bar{s}) \tag{55}$$

In the FEM, the tether degrees of freedom are taken as the actual values of displacements, slopes, or curvatures at points along the tether (nodes), and the shape functions are chosen as interpolation functions for the tether degrees of freedom. This representation is different from the AMM in that the degrees of freedom in the AMM are arbitrary generalized coordinates that have no obvious physical interpretation. Expanding the left-hand side of Eq. (47) as in Eq. (25) and introducing Eqs. (53–55), the tether equations of motion are written as

$$\begin{aligned} \sum_{j=1}^{n} M_{ij} \ddot{C}_{1j} = &- \sum_{j=1}^{n} M_{ij} [-2\omega_{EN3}\dot{C}_{2j} + 2\omega_{EN2}\dot{C}_{3j} \\ &- (\omega_{EN2}^2 + \omega_{EN3}^2) C_{1j} + (\omega_{EN1}\omega_{EN2} - \dot{\omega}_{EN3}) C_{2j} \\ &+ (\dot{\omega}_{EN2} + \omega_{EN1}\omega_{EN3}) C_{3j}] - (\dot{\omega}_{EN2} + \omega_{EN1}\omega_{EN3})\gamma_{4i} \\ &- \gamma_{1i}\ddot{r}_{A1} - \gamma_{2i}\ddot{p}_{A1} + \gamma_{3i}\ddot{p}_{B1} + g_{i1} + f_{i1} \end{aligned} \tag{56}$$

$$\sum_{j=1}^{n} M_{ij}\ddot{C}_{2j} = -\sum_{j=1}^{n} M_{ij}[2\omega_{EN3}\dot{C}_{1j} - 2\omega_{EN1}\dot{C}_{3j} + (\dot{\omega}_{EN3} + \omega_{EN1}\omega_{EN2})C_{1j} - (\omega_{EN1}^2 + \omega_{EN3}^2)C_{2j} + (\omega_{EN2}\omega_{EN3} - \dot{\omega}_{EN1})C_{3j}] - (\omega_{EN2}\omega_{EN3} - \dot{\omega}_{EN1})\gamma_{4i} - \gamma_{1i}\ddot{r}_{A2} - \gamma_{2i}\ddot{p}_{A2} + \gamma_{3i}\ddot{p}_{B2} + g_{i2} + f_{i2} \tag{57}$$

$$\sum_{j=1}^{n} M_{ij}\ddot{C}_{3j} = -\sum_{j=1}^{n} M_{ij}[-2\omega_{EN2}\dot{C}_{1j} + 2\omega_{EN1}\dot{C}_{2j} + (\omega_{EN1}\omega_{EN3} - \dot{\omega}_{EN2})C_{1j} + (\dot{\omega}_{EN1} + \omega_{EN2}\omega_{EN3})C_{2j} - (\omega_{EN1}^2 + \omega_{EN2}^2)C_{3j}] + (\omega_{EN1}^2 + \omega_{EN2}^2)\gamma_{4i} - \gamma_{1i}\ddot{r}_{A3} - \gamma_{2i}\ddot{p}_{A3} + \gamma_{3i}\ddot{p}_{B3} + g_{i3} + f_{i3} \tag{58}$$

for $i = 1, \ldots, n$, where ω_{ENj}, r_{Aj}, p_{Aj}, p_{Bj}, g_{ij}, and f_{ij} are the jth components of their respective vectors expressed in $\mathcal{F}_E$. In Eqs. (56–58), we have also introduced

$$M_{ij} = \int_0^L N_i(\bar{s})N_j(\bar{s})\,\mathrm{d}\bar{s} + \frac{m_B}{\bar{\rho}}N_i(L)N_j(L) \tag{59}$$

$$\gamma_{4i} = \int_0^L \bar{s}N_i(\bar{s})\,\mathrm{d}\bar{s} + \frac{m_B L}{\bar{\rho}}N_i(L) \tag{60}$$

Equations (56–58) define a set of $3n$ ODEs for the tether degrees of freedom. These ODEs, when solved in combination with the ODEs governing the motion of the end bodies and the tether librations, give a complete solution for the motion of the EDT system.

To assemble Eqs. (56–58), the tether is partitioned into N_e uniform finite elements. We desire continuity of displacement and slope at the element interfaces, and so two-node elements are used with displacement and slope at the nodes as degrees of freedom. Thus, $n = 2(N_e + 1)$ and there are $6(N_e + 1)$ total degrees of freedom for the discretized equations of motion. Defining the element natural coordinate $\xi \in [0, 1]$ as

$$\xi = \frac{\bar{s} - \bar{s}_0}{\bar{s}_f - \bar{s}_0} = \frac{\bar{s} - \bar{s}_0}{\ell_e} \tag{61}$$

the shape functions for a single element are the cubic Hermite interpolation polynomials:

$$N_1^e = 1 - 3\xi^2 + 2\xi^3 \tag{62}$$

$$N_2^e = \xi - 2\xi^2 + \xi^3 \tag{63}$$

$$N_3^e = 3\xi^2 - 2\xi^3 \tag{64}$$

$$N_4^e = -\xi^2 + \xi^3 \tag{65}$$

Using these functions, the displacement over an element (take u, for example) is written as

$$u^e(\xi, t) = u_1(t)N_1^e(\xi) + \frac{\mathrm{d}u_1(t)}{\mathrm{d}\xi}N_2^e(\xi) + u_2(t)N_3^e(\xi) + \frac{\mathrm{d}u_2(t)}{\mathrm{d}\xi}N_4^e(\xi) \tag{66}$$

where u_i is the displacement at the ith node of the element. Also note that because of the way the element shape functions are defined, C_{ij} denotes tether displacements when j is odd and slopes when j is even. Substituting Eq. (66) into Eqs. (56–58) and applying principles of finite element assemblage [20], the full equations of motion for the tether vibrations are obtained. The boundary conditions of the tether are applied to these equations by forcing $C_{i1} = 0$, $C_{1,n-1} = C_{2,n-1} = 0$, and $\ddot{C}_{3,n-1} = \ddot{w}(L, t)$ for all time.

III. Code Verification

Because the equations governing the tether vibrations are PDEs and therefore must be converted to a finite set of ODEs to obtain a numerical solution, we would like a rigorous method of determining whether the computer codes written to solve the discretized equations of motion produce accurate solutions. If they do, then they also produce accurate approximate solutions to the original PDEs, provided that the discretization is sufficiently fine. One possible approach to addressing this problem for systems such as the EDT system considered in this work is to include the total system energy as an additional state and to ensure that the values predicted by numerical integration agree with values calculated using the state time history after numerical integration. In this paper, we use a more rigorous method that is more commonly used in the field of computational fluid dynamics: the MMS [17,18].

The idea of the MMS is that an exact solution to a modified set of PDEs can be manufactured by introducing additional terms into the equations of motion and boundary conditions of the original system. The modified PDEs and boundary conditions are discretized and solved numerically, and the manufactured solution is used to determine errors for approximate solutions calculated at increasing levels of discretization refinement. These errors should decrease toward zero as the discretization is refined. For some discretization methods, such as the FEM, we even know the rate at which these errors should decrease. If the errors decrease as expected, then the terms introduced to form the modified equations can simply be removed from the computer codes used to generate the numerical solution, and we know that the numerical solutions to the original PDEs are accurate provided that the discretization is sufficiently fine.

The MMS is applied to the EDT system by modifying Eq. (17) and the $\mathcal{B}$ equation of motion (which defines the dynamic boundary condition of the tether):

$$\ddot{\mathbf{r}} = -\frac{\mu}{\|\mathbf{R}_T\|^3}\mathbf{R}_T + \frac{1}{\bar{\rho}}\frac{\partial \mathbf{T}}{\partial \bar{s}} + \frac{i}{\bar{\rho}}\frac{\partial \mathbf{r}}{\partial \bar{s}} \times \mathbf{B} - \ddot{\mathbf{r}}_A - \ddot{\mathbf{p}}_A + \mathbf{f}_T \tag{67}$$

$$m_B\ddot{\mathbf{r}}_B = -\frac{m_B\mu}{\|\mathbf{r}_B\|^3}\mathbf{r}_B - \mathbf{T}(L, t) + \mathbf{f}_L \tag{68}$$

where $\mathbf{f}_T$ and $\mathbf{f}_L$ are the terms introduced to create the manufactured solution. A solution is assumed for $\mathbf{r}(\bar{s}, t)$ and the tether libration angles, and the values of $\mathbf{f}_T$ and $\mathbf{f}_L$ required to produce the assumed solution are solved for. The modified PDEs are then discretized according to the previous section, and numerical solutions for the EDT system motion are obtained. As the discretization is refined by increasing the number of assumed modes or finite elements, the errors between the numerical and manufactured exact solutions should decrease toward zero. In the next two subsections, we apply the preceding procedure to the FEM and AMM.

A. Finite Element Method

Let F represent the exact solution to the modified PDEs, and let f represent the numerical solution determined for a certain number of finite elements. Note that F is known because we have manufactured an exact solution to the modified PDEs. For the FEM, the discretization error of the numerical solution is calculated using the discrete l^2-norm:

$$\epsilon = \sqrt{\frac{1}{N}\sum_{j=1}^{N}(f_j - F_j)^2} \tag{69}$$

where the summation is over all points in space and time in the solution domain, and a subscript j indicates a value evaluated at the jth point in the solution domain. The discretization error can be expressed as

$$\epsilon = C_{\Delta h}\Delta h^p + C_{\Delta t}\Delta t^q + \text{H.O.T} \tag{70}$$

where H.O.T represents higher-order terms in Δh and Δt. If the numerical solution is in the asymptotic solution range, then the higher-order terms are negligible, and we have

$$\epsilon = C_{\Delta h}\Delta h^p + C_{\Delta t}\Delta t^q \tag{71}$$

Further, if we know that the error due to the temporal discretization is insignificant relative to the spatial discretization error, then we can simply write the discretization error as

$$\epsilon = C_{\Delta h}\Delta h^p \tag{72}$$

The temporal discretization error will be negligible for situations in which highly accurate time integrators are used with tight integration tolerances (for example, most of the built-in MATLAB ODE solvers, which use variable time steps and allow for very tight tolerances to minimize temporal discretization error). Given two numerical solutions with discretization errors ϵ_1 and ϵ_2, an observed order of accuracy can be calculated using Eq. (72) as

$$p = \frac{\ell_n(\epsilon_1/\epsilon_2)}{\ell_n(r)} \tag{73}$$

where the refinement factor $r = N_{e2}/N_{e1}$ provides a measure of the relative level of refinement between the two numerical solutions. If the FEM discretization computer code is accurately solving the discretized equations of motion, then p determined from Eq. (73) will converge to the theoretical order of accuracy of the method as the number of finite elements in increased.

The manufactured solution used for the FEM in this work is

$$u^*(\bar{s}, t) = A_1 \sin(2t)\sin\left(\frac{\pi}{L}\right) \tag{74}$$

$$v^*(\bar{s}, t) = A_2 \sin(t)\sin\left(\frac{\pi}{L}\right) \tag{75}$$

$$w^*(\bar{s}, t) = A_3 \cos(t)\left(\frac{\bar{s}}{L}\right)^3 \tag{76}$$

$$\alpha^*(\bar{s}, t) = A_4 \cos\left(\frac{\sqrt{\mu l}}{r_A^2}t\right) \tag{77}$$

$$\beta^*(\bar{s}, t) = A_5 \cos\left(2\frac{\sqrt{\mu l}}{r_A^2}t\right) \tag{78}$$

where r_A and l are instantaneous values. Note that it is not necessary to chose a physically realistic manufactured solution. All that is required is that the solution be smooth with smooth derivatives and that no derivatives vanish [17]. In fact, it can be beneficial to chose an unrealistic manufactured solution, because, as is the case with the EDT system, much shorter simulation times can be used to capture the important behavior of the solution. When applying the MMS to any system, care must be taken to ensure that the initial conditions of any simulation agree with the manufactured solution. Thus, the initial conditions for the tether motion are determined by setting $t = 0$ in Eqs. (74–78).

The MMS terms $\mathbf{f}_T$ and $\mathbf{f}_L$ are calculated numerically, and the integral terms containing $\mathbf{g}_i$, $\mathbf{f}_i$, $\mathbf{f}_T$, and $\mathbf{f}_L$ are evaluated numerically using Simpson's rule with 101 evaluation points per finite element. The number of points was determined to be sufficient to render the error due to the numerical integration using Simpson's rule negligible relative to the discretization error. The discretized equations of motion are numerically integrated using the built-in MATLAB function `ode15s`, which is designed to integrate stiff systems of ODEs and differential algebraic equations. The function `ode15s` uses a variable-order method based upon numerical differentiation formulas. Both the absolute and relative integration tolerances are set to 10^{-12} for all simulations. These tight tolerances ensure that round-off errors and iterative convergence errors that accumulate during numerical integration do not have a significant impact on the discretization error and thus on the observed order of accuracy. The constants for the manufactured solution are taken as $A_1 = 50$, $A_2 = 25$, $A_3 = 10$, $A_4 = 2\pi/180$, and $A_5 = \pi/180$, and the system parameters used in the simulations are shown in Table 1. The simulation time is 2π s. This may seem like a short simulation time for an EDT system, but the periods of the manufactured tether displacements are all on the order of 2π s. Thus, although the integration time would be short for a simulation of the actual motion of an orbiting EDT system, it is sufficient to determine discretization errors and observed orders of accuracy for the manufactured solution used in this study. Simulations are performed using 2–32 finite elements with a refinement factor of $r = 2$.

Table 1 EDT system parameters used in MMS simulations

System parameter	Value
Unstretched length L, m	20,000
Modulus of elasticity E, N/m^2	70×10^9
Unstretched diameter d, mm	1
Unstretched linear mass density $\bar{\rho}$, kg/m	0.0025
Structural damping constant c, s	0.06
Body A mass m_A, kg	500
Body B mass m_B, kg	50
Body A inertias $\boldsymbol{I}_A$, kg $\cdot$ m^2	diag[300 400 200]
Body B inertias $\boldsymbol{I}_B$, kg $\cdot$ m^2	diag[30 40 20]
Body A attachment vector $\boldsymbol{p}_A$, m	[0 0 1]
Body B attachment vector $\boldsymbol{p}_B$, m	[0 0 −0.1]
Current i, A	1

Figures 2 and 3 show the discretization errors and observed orders of accuracy for the tether displacements calculated from the simulations. Numerical values are listed in Table 2. The discretization errors for each displacement decrease at roughly equal rates as the number of finite elements is increased, indicating that they all have the same order of accuracy. The observed orders of accuracy confirm this observation, as the orders of accuracy converge to a value of 4 for all three displacements. Because the FEM discretization we used employs cubic shape functions, it has a theoretical order of accuracy of 4 [21]. Thus, the observed order of accuracy of the numerical simulations matches the theoretical value. This means that we can be confident that the FEM computer code is accurately solving the discretized equations of motion and that numerical solutions to the original set of PDEs are accurate provided that enough finite elements are used.

B. Assumed Modes Method

A slightly different approach is used to apply the MMS to the AMM. With the FEM, we were able to perform an element refinement study and determine observed orders of accuracy. These orders of accuracy converged to the theoretical value of the FEM

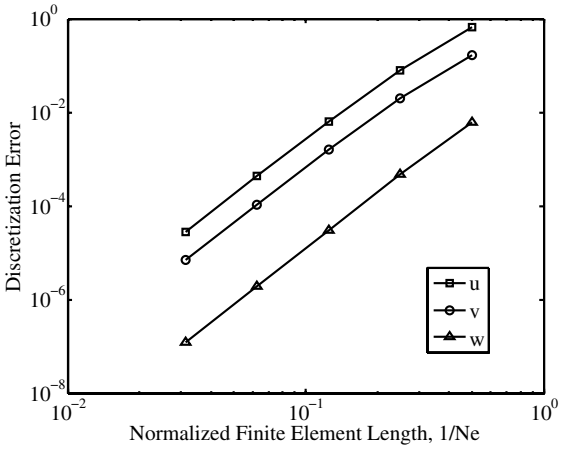

Fig. 2 Discretization error as a function of normalized finite element length.

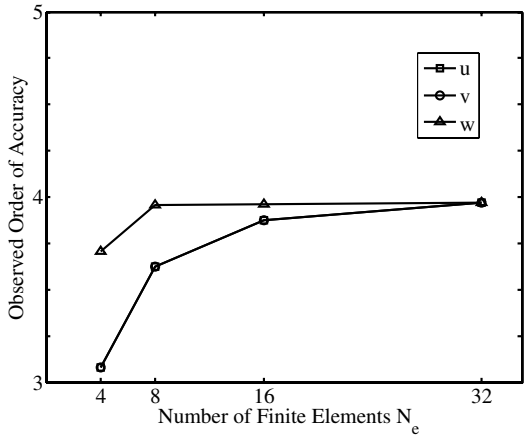

Fig. 3 Observed order of accuracy as a function of number of finite elements.

discretization as the number of finite elements was increased, thus validating the finite element discretization. With the AMM, we take advantage of the structure of the assumed solution form for the tether displacements to create a scenario in which the solution to the discretized equations of motion is *exactly* the manufactured solution. The numerical solution should then match the manufactured solution with a high degree of accuracy, and the agreement should improve as the integral terms in the right-hand sides of the discretized equations of motion are evaluated more accurately.

Recall that in the AMM, the tether displacements are assumed to be of the form

$$u(\bar{s},t)=\sum_{j=1}^{N_T} C_{1j}\sqrt{2}\sin\left(\frac{j\pi}{L}\bar{s}\right) \tag{79}$$

$$v(\bar{s},t)=\sum_{j=1}^{N_T} C_{2j}\sqrt{2}\sin\left(\frac{j\pi}{L}\bar{s}\right) \tag{80}$$

$$w(\bar{s},t)=\sum_{j=1}^{N_T} C_{3j}\left(\frac{\bar{s}}{L}\right)^{j} \tag{81}$$

Now let the manufactured solution for the tether displacements be

$$u^*(\bar{s},t)=A_1\sin(2t)\left[\sin\left(\frac{\pi}{L}\bar{s}\right)+\sin\left(\frac{3\pi}{L}\bar{s}\right)\right] \tag{82}$$

Table 2 Finite element discretization refinement results

Elements	Discretization error	Error ratio	Observed accuracy
	u displacement		
2	0.66076950	——	——
4	0.07812766	8.45756182	3.08024182
8	0.00633334	12.33592802	3.62479435
16	0.00043225	14.65220335	3.87304572
32	0.00002758	15.67135128	3.97005768
	v displacement		
2	0.16512387	——	——
4	0.01953099	8.45445561	3.07971186
8	0.00158330	12.33562141	3.62475849
16	0.00010808	14.64985584	3.87281456
32	0.00000690	15.65400028	3.96845947
	w displacement		
2	0.00612407	——	——
4	0.00046950	13.04385461	3.70529836
8	0.00003027	15.50906066	3.95503940
16	0.00000194	15.58361089	3.96195766
32	0.00000012	15.67354582	3.97025969

$$v^*(\bar{s},t)=A_2\sin(t)\left[\sin\left(\frac{\pi}{L}\bar{s}\right)+\sin\left(\frac{2\pi}{L}\bar{s}\right)\right] \tag{83}$$

$$w^*(\bar{s},t)=A_3\cos(t)\left[\left(\frac{\bar{s}}{L}\right)-\left(\frac{\bar{s}}{L}\right)^2+\left(\frac{\bar{s}}{L}\right)^3\right] \tag{84}$$

The manufactured solutions for the tether libration angles are the same as those used with the FEM. Comparing Eqs. (79–81) with Eqs. (82–84), we can see that for $N_T, N_L \geq 3$, the solution to the discretized equations of motion should match the manufactured solution with

$$C_{11}(t)=C_{13}(t)=\frac{A_1\sin(2t)}{\sqrt{2}} \tag{85}$$

$$C_{12}(t)=0 \tag{86}$$

$$C_{21}(t)=C_{22}(t)=\frac{A_2\sin(t)}{\sqrt{2}} \tag{87}$$

$$C_{23}(t)=0 \tag{88}$$

$$C_{31}(t)=C_{33}(t)=A_3\cos(t) \tag{89}$$

$$C_{32}(t)=-A_3\cos(t) \tag{90}$$

There will be some error due to round-off and the fact that the integral terms in the discretized equations of motion must be evaluated numerically, but these errors should decrease as the integral terms are evaluated more accurately.

The right-hand sides of the AMM discretized equations of motion (all of the inertia, gravity, electrodynamic force, and MMS terms) are calculated numerically using Simpson's rule. As with the FEM, the MATLAB function `ode15s` is used to numerically integrate the discretized equations of motion with absolute and relative tolerances of 10^{-12}. The constants for the manufactured solution are $A_1=50$, $A_2=25$, $A_3=10$, $A_4=2\pi/180$, and $A_5=\pi/180$, and the remaining system parameters are the same as those used in the FEM study. Once again, the simulation time is 2π s. Simulations are performed for different numbers of evaluation points used to calculate the integral terms in the right-hand sides of the discretized equations of motion, and errors between the numerical and exact solutions are determined.

The errors between the numerical and exact solutions are plotted in Fig. 4. For all three displacements, the difference between the numerically calculated coefficients and the exact solution values decrease as the number of evaluation points is increased before leveling off around steady values. This convergence is most likely due to round-off errors and iterative convergence errors that arise during numerical integration. The steady values reached by all three displacements are on the order of 10^{-9}, which is equivalent to an error of approximately $10^{-9}\%$ between the numerical and exact solutions. As we determined with the FEM, the computer code that implements the AMM discretization accurately solves the discretized equations of motion, and we can be confident that numerical solutions for the original set of PDEs are accurate as long as enough assumed modes are used.

IV. Comparison of Discretization Methods

The computer codes that implement the AMM and the FEM both work well for low numbers of assumed modes or finite elements, in that both produce numerical solutions in a relatively short computational time. However, as the number of assumed modes used to approximate the longitudinal vibrations increases, the computational time for the AMM increases rapidly, rendering the method

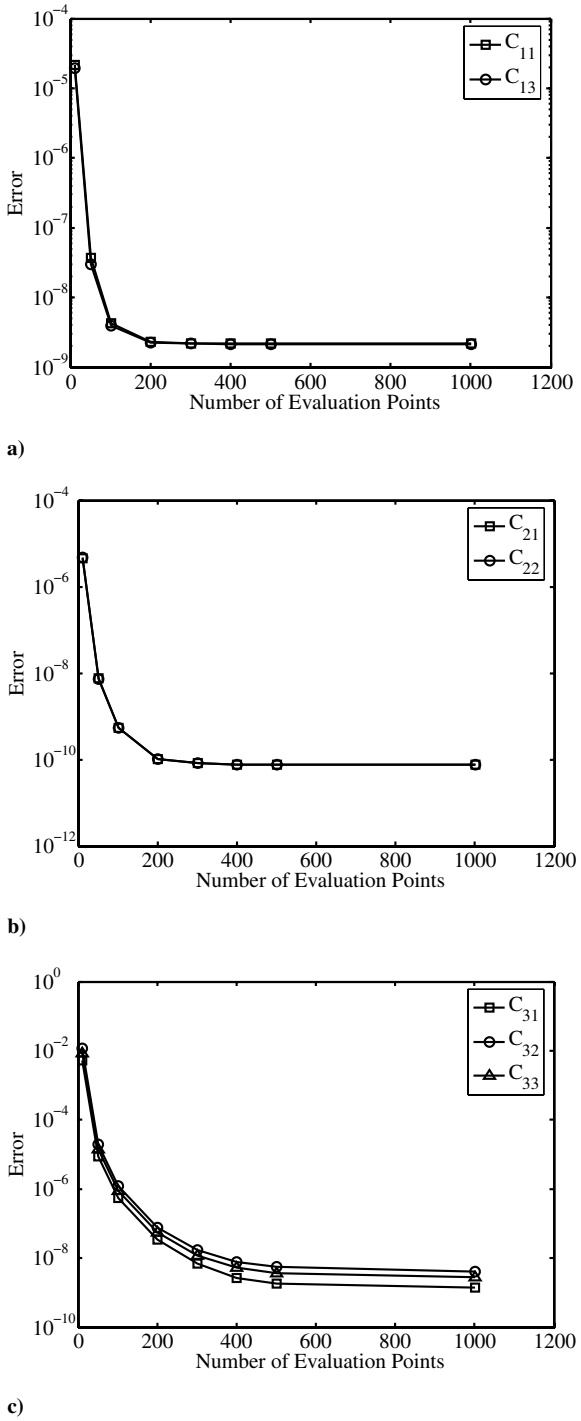

Fig. 4 Error between numerical and exact solutions for a) *u* displacement, b) *v* displacement, and c) *w* displacement generalized coordinates.

practically useless. To see why this happens, consider the elements of Eqs. (40) and (41), which form the mass matrix for the longitudinal vibrations. As N_L increases, the columns of the longitudinal mass matrix become increasingly similar, causing the mass matrix to become nearly singular. This nearly singular behavior introduces significant numerical errors into the calculation of the accelerations of the longitudinal degrees of freedom, because the inverse of the mass matrix is used in their calculations, and these errors in the accelerations can actually cause the longitudinal vibrations to diverge when they should not. As the time integrator attempts to compensate for this divergent behavior, the time steps become very small and the total integration time becomes prohibitively large. The FEM does not have this same problem because the diagonal structure of the system mass matrices ensures that their columns always linearly independent, and so there are no problems in taking their inverses due to ill-conditioning.

Nearly singular behavior of the system mass matrix for simple polynomial shape functions in the AMM has been reported previously [22], and the simplest method of eliminating the problem is to use a different set of assumed mode functions for the longitudinal vibrations. The best possible set would be an orthogonal set that would make the mass matrix diagonal and trivially invertible. Another possibility would be to use the mode shapes for the longitudinal vibrations of a similar, but much simpler, problem as the longitudinal assumed mode functions. These mode shapes would be orthogonal or nearly orthogonal, and the resulting mass matrix would always have well-defined inverses. Other possible sets of longitudinal assumed mode functions exist, but their analysis and implementation is left for future work.

Another advantage of the FEM over the AMM not specific to the shape functions used in the AMM is that initial conditions are much easier to set in the FEM. Because the degrees of freedom in the FEM are simply displacements and slopes at points along the tether, any arbitrary initial tether shape can be trivially converted to a set of initial coordinates for numerical integration. This is not the case with the AMM, in which determining a set of coordinates from an arbitrary tether shape requires a process similar to calculating the coefficients of a Fourier series. Although this is not necessarily a difficult task, it is more involved than the process required in the FEM.

V. Conclusions

The method of manufactured solutions (MMS) provides a rigorous and relatively simple means of verifying computer codes written to numerically integrate the equations of motion for an electrodynamic tether (EDT) system. The main advantage of the MMS over other methods of code verification, such as using work-energy relations to monitor the total system energy, is that the MMS uses a modified set of equations of motion with a known exact solution. Because this solution is known, whether solutions produced by the code converge to the solution as expected as the discretization is refined is unambiguous.

The MMS was used to verify computer codes that integrate the EDT system equations of motion using the finite element method (FEM) and the assumed modes method (AMM) for spatial discretization of the tether equations. For low numbers of assumed modes or finite elements, both the AMM and the FEM codes produce numerical solutions in relatively short computational times. However, as the number of longitudinal assumed modes used in the AMM increases, the mass matrix for the longitudinal degrees of freedom becomes nearly singular, and the integration time becomes prohibitively high. This behavior is not seen in the FEM, making the FEM a much better choice than the AMM presented in this work for systems requiring a high level of discretization refinement. The FEM has other, more general, advantages over the AMM, such as the relative ease of setting initial conditions and the easy physical interpretation of the degrees of freedom. For all of these reasons, the FEM is better suited to the dynamic simulation of electrodynamic tether systems.

References

[1] Forward, R., Hoyt, R., and Uphoff, C., "Terminator Tether™: A Spacecraft Deorbit Device," *Journal of Spacecraft and Rockets*, Vol. 37, No. 2, 2000, pp. 187–196. doi:10.2514/2.3565

[2] Iess, L., Bruno, C., Ulivieri, C., Ponzi, U., Parisse, M., Laneve, G., Vannaroni, G., Dobrowolny, M., Venuto, F. D., Bertotti, B., and Anselmo, L., "Satellite De-Orbiting by Means of Electrodynamic Tethers Part 1: General Concepts and Requirements," *Acta Astronautica*, Vol. 50, No. 7, 2002, pp. 399–406. doi:10.1016/S0094-5765(01)00180-1

[3] Bruno, L. I. C., Ulivieri, C., and Vannaroni, G., "Satellite De-Orbiting by Means of Electrodynamic Tethers Part 2: System Configuration and Performance," *Acta Astronautica*, Vol. 50, No. 7, 2002, pp. 407–416. doi:10.1016/S0094-5765(01)00181-3

[4] Vas, I., Kelly, T., and Scarl, E., "Space Station Reboost with Electrodynamic Tethers," *Journal of Spacecraft and Rockets*, Vol. 37, No. 2, 2000, pp. 154–164. doi:10.2514/2.3559

[5] Bonometti, J., Sorensen, K., Dankanich, J., and Frame, K., "2006 Status of the Momentum eXchange Electrodynamic Re-Boost (MXER) Tether Development," 42nd AIAA/ASME/SAE/ASEE Joint Propulsion Conference and Exhibit, AIAA Paper 2006-4521, Sacramento, CA, 2006.

[6] Tragesser, S., and San, H., "Orbital Maneuvers with Electrodynamic Tethers," *Journal of Guidance, Control, and Dynamics*, Vol. 26, No. 5, 2003, pp. 805–810. doi:10.2514/2.5115

[7] Williams, P., "Optimal Orbital Transfer with Electrodynamic Tether," *Journal of Guidance, Control, and Dynamics*, Vol. 28, No. 2, 2005, pp. 369–372. doi:10.2514/1.12016

[8] Pelaez, J., Ruiz, M., Lopez-Rebollal, O., Lorenzini, E., and Cosmo, M., "A New Kind of Dynamic Instability in Electrodynamic Tethers," *Journal of the Astronautical Sciences*, Vol. 48, No. 4, 2000, pp. 449–476.

[9] Pelaez, J., Ruiz, M., Lopez-Rebollal, O., Lorenzini, E. C., and Cosmos, M. L., "Two-Bar Model for the Dynamics and Stability of Electrodynamic Tethers," *Journal of Guidance, Control, and Dynamics*, Vol. 25, No. 6, 2002, pp. 1125–1135. doi:10.2514/2.4992

[10] Somenzi, L., Iess, L., and Pelaez, J., "Linear Stability Analysis of Electrodynamic Tethers," *Journal of Guidance, Control, and Dynamics*, Vol. 28, No. 5, 2005, pp. 843–849. doi:10.2514/1.11822

[11] Beletsky, V., and Levin, E., *Dynamics of Space Tether Systems*, Univelt, San Diego, CA, 1993, Chap. 5.

[12] Levin, E., *Dynamic Analysis of Space Tether Missions*, Univelt, San Diego, CA, 2007, Chap. 4.

[13] Ellis, J., and Hall, C., "Dynamics of an Electrodynamic Tether System Including Gyrostat End Bodies," *Advances in the Astronautical Sciences*, Vol. 127, No. 2, 2007, pp. 1331–1350.

[14] Ruiz, M., Lopez-Rebollal, O., Lorenzini, E., and Pelaez, J., "Modal Analysis of the Stability of Periodic Solutions in Electrodynamic Tethers," *Advances in the Astronautical Sciences*, Vol. 109, Pt. 2, 2001, pp. 1553–1570.

[15] Pradhan, S., Modi, V., and Misra, A., "On the Offset Control of Flexible Nonautonomous Tethered Two-Body Systems," *Acta Astronautica*, Vol. 38, No. 10, 1996, pp. 783–801. doi:10.1016/S0094-5765(96)00080-X

[16] Steiner, W., Steindl, A., and Troger, H., "Dynamics of a Space Tethered Satellite System with Two Rigid End Bodies," *Fourth International Conference on Tethers in Space*, Smithsonian Inst., Washington, D.C., 1995, pp. 1367–1379.

[17] Roy, C., "Review of Code and Solution Verification Procedures for Computational Simulation," *Journal of Computational Physics*, Vol. 205, No. 1, 2005, pp. 131–156. doi:10.1016/j.jcp.2004.10.036

[18] Roache, P., *Verification and Validation in Computational Science and Engineering*, Hermosa, Albuquerque, NM, 1998, Chap. 3.

[19] Meirovitch, L., *Elements of Vibration Analysis*, McGraw–Hill, New York, 1975, pp. 523–529.

[20] Huebner, K., Thornton, E., and Byrom, T., *The Finite Element Method for Engineers*, 3rd ed., Wiley, New York, 1995, pp. 214–232.

[21] Axelsson, O., and Barker, V., *Finite Element Solution of Boundary Value Problems*, Academic Press, Inc., Orlando, FL, 1984, pp. 214–232.

[22] Singhvi, S., and Kapania, R., "Comparison of Simple and Chebychev Polynomials in Rayleigh-Ritz Analysis," *Journal of Engineering Mechanics*, Vol. 120, No. 10, 1994, pp. 2126–2135. doi:10.1061/(ASCE)0733-9399(1994)120:10(2126)